

Active Lubrication of Transluminal Medical Instruments

Mostafa A. Atalla^{1,2*}, Jelte Nieuwenhuis¹, Alan Martin³, Xuan Wang³,
Ahranee Candan³, Matt J. Carré³, Roger Lewis³, Aimée Sakes^{†1},
Michaël Wiertlewski^{†2}

¹Department of BioMechanical Engineering, TU Delft, Delft, The Netherlands.

²Department of Cognitive Robotics, TU Delft, Delft, The Netherlands.

³The School of Mechanical, Aerospace and Civil Engineering, University of Sheffield,
Sheffield United Kingdom.

*Corresponding author(s). E-mail(s): m.a.a.atalla@tudelft.nl;

Abstract

Transluminal minimally invasive surgery uses natural orifices and small incisions to access internal anatomical structures, promoting quicker recovery and reduced morbidity. However, navigating instruments—catheters and endoscopes—through anatomical pathways creates frictional interactions with luminal walls, risking complications such as perforation, poor haptic feedback, and instrument buckling. In this paper, we present a new approach to actively lubricate transluminal instruments and dynamically reduce friction with surrounding tissues. This approach employs ultrasonic vibrations, at the instrument surface, to generate a pressurized fluid layer at the contact interface, lubricating the interface and thereby reducing friction. We implemented this approach in a prototype catheter, which we validated under dry and liquid-lubricated conditions, across rigid and soft interfaces, and along varied anatomical curvatures. In a cardiac catheter use case, active lubrication reduced friction by up to **42%** on ex-vivo porcine aorta tissue and **82%** on rigid substrates, denoting its potential performance on healthy and calcified tissue, respectively. Thermal imaging confirmed that temperature at the tissue-catheter interface remained within safe limits. Additionally, the system effectively prevented buckling during catheter insertion experiment, further showcasing its potential. By minimizing injury risk and enhancing procedural stability, active lubrication can drastically enhance the safety and efficacy of transluminal interventions.

Keywords: Minimally Invasive Transluminal Surgery, Transluminal Medical Instruments, Catheter Technology, Ultrasonic Lubrication, Friction Modulation, Friction Control, Biotribology

Introduction

Minimally invasive surgeries have reshaped healthcare by reducing patient trauma, shortening recovery time, and improving clinical outcomes. Among these techniques, transluminal interventions—which access internal anatomy through

natural orifices and small incisions—are significantly less invasive than alternative surgeries such as open surgery, enabling intricate procedures at difficult-to-reach anatomical targets[1, 2, 3]. These interventions typically follow a two-phase structure: first, the instruments navigate along anatomical pathways toward the target and, second, once the instrument is positioned, surgical

[†]A. Sakes and M. Wiertlewski are co-senior authors.

tasks are performed at the target site. Because tissue interaction differs markedly between these phases, the design of transluminal instruments must accommodate contrasting functional requirements. In particular, friction must be low during insertion for smooth navigation and minimal tissue damage, yet needs to remain high when the instrument is at the target location for stability.

During navigation, the insertion of transluminal instruments, such as catheters and endoscopes, causes frictional interactions with surrounding tissue [4, 5], as illustrated in Fig. 1(a). This friction can result in tissue damage, bleeding, and patient discomfort. Such complications are evident in different transluminal procedures such as catheterization [6, 7, 8, 9, 10, 11], colonoscopy [12, 13, 14], and upper gastrointestinal endoscopy [15, 16, 17]. In addition to tissue damage, friction diminishes haptic transparency and alters the interventionist’s force perception, thereby increasing the risk of accidental dissection or perforation [18, 19, 20]. Excessive friction can also cause flexible transluminal instruments to buckle (Fig. 1b). While buckling, the instrument shaft can suddenly release the stored elastic energy, exerting intense forces which can potentially result in catastrophic damage to the luminal wall [21, 22]. In robot-assisted interventions, buckling further complicates control and often necessitates additional mechanical stabilization [23, 24]. In the example of transluminal catheterization procedures, as illustrated in Fig. 1(b), excessive friction can damage the vessel walls, promoting post-operative thrombus formation. High friction may also cause disintegration of calcified particles, some of which can subsequently travel through the bloodstream and potentially obstruct critical vessels.

However, while high friction is detrimental to the navigation of transluminal instruments, it becomes an asset when executing surgical operations such as cutting, puncturing, or suturing. All these operations require frictional anchoring between the instrument and the tissue in order to maintain position and apply force with precision [25, 26, 27]. In low-friction conditions, particularly within open cavities such as the heart, the instability of the instrument may hinder effective manipulation and compromise procedural success (Fig. 1c). This contradiction, where low friction is needed during navigation and high friction is needed when anchoring, is a significant design

challenge for instruments coating, which must strike a balance between ease of navigation and stability.

In transluminal interventions, lubrication is typically passive and remains uncontrollable throughout the procedure. Conventional strategies to minimize tissue damage during instrument movement rely on liquid lubricants [28, 29, 30, 31, 32] or self-lubricating coatings, such as hydrophilic coatings that become slippery when exposed to a wet surface [33, 34]. However, these methods have notable limitations. Add-on lubricants are often short-lived, gradually losing effectiveness as they are wiped away during navigation [28]. Hydrophilic coatings, though effective in specific procedures such as urology, lack versatility for broader transluminal applications. Crucially, neither approach offers dynamic control over friction—they cannot switch between low-friction and high-friction states based on the procedural phase. As a result, instruments with fixed frictional properties are suboptimal for interventions that require smooth navigation followed by precise and stable task execution. Considering the critical role of friction in transluminal interventions, we urgently need new methods that enable real-time, on-demand friction control.

This paper introduces to transluminal instruments, an active lubrication concept, enabling real-time control of friction via ultrasonic lubrication. By dynamically switching between low and high friction states, the instrument can navigate safely to its destination and then transition to a stable configuration for surgical tasks. Ultrasonic lubrication uses high-frequency surface vibrations to create a pressurized squeeze film of fluid at the interface between the instrument and tissue. This fluid film forms through nonlinear compression of the fluid trapped at the interface, producing a fluid cushion that levitates the vibrating surface away from the counter surface—a phenomenon known as squeeze-film levitation. At the microscopic level, this levitation disengage the surface roughness asperities from direct contact, thereby reducing friction during sliding motion, such as during navigation. Friction decreases monotonically with the amplitude of vibration, therefore friction can be easily controlled on-demand [35, 36]. Ultrasonic lubrication has enabled novel innovations in tactile displays [37], contactless manipulation

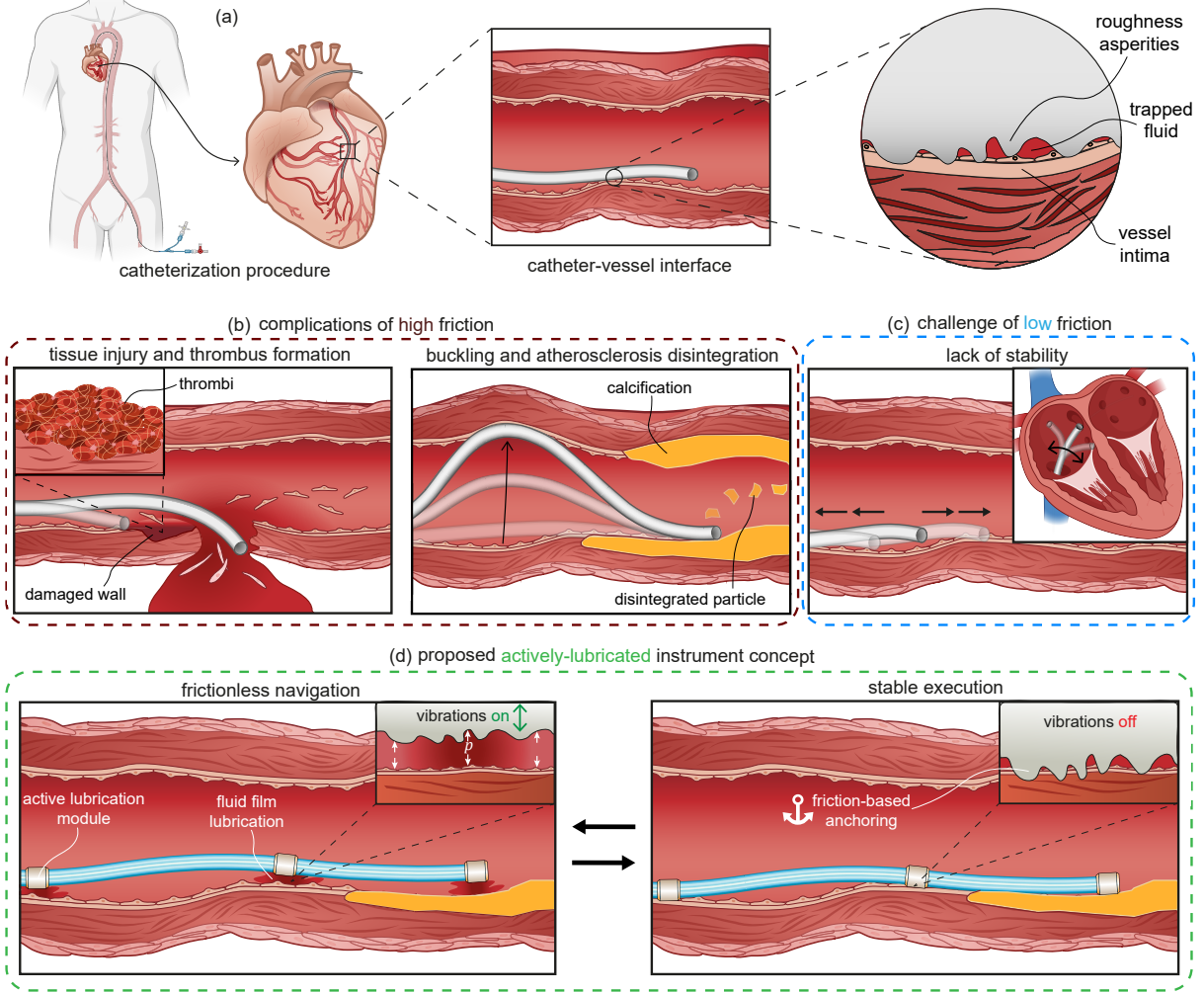


Fig. 1 Our approach mitigates friction-induced complications and challenges in catheterization procedures.

(a) During a typical cardiac procedure, a catheter is inserted through the femoral artery and navigates to the heart where the intervention is performed. The magnified view shows the catheter-vessel interface on a microscopic level. At this scale the asperities of the catheter body are in intimate contact with the vessel wall. (b) High friction with the catheter can perforate and degrade the vessel wall, increasing the risk of post-operative thrombus formation. Additionally, excessive friction in calcified regions may cause the catheter to buckle, exerting excessive forces on the vessel wall and potentially disintegrating atherosclerotic particles, which pose a serious risk if they migrate through the bloodstream. (c) Low friction between catheter and blood vessel causes poor stability, increasing movement variability and reducing precision. (d) Catheter with active lubrication uses discrete friction control modules along its shaft to dynamically change friction during the operation. These module use ultrasonic transverse vibrations to create a pressurized fluid film at the interface, which disengage the roughness asperities away from the luminal wall, drastically reducing the intimate contact and enabling frictionless navigation. Once the catheter reaches its region of interest, vibrations can be turned off, which causes the modules to return in contact with the vessel wall, anchoring them with frictional contact. Simply turning the vibration on and off, switches between the high- and low-friction states.

[38], and squeeze-film bearings [39, 40]. While these applications rely on the compressibility of air to modulate friction, we recently proved that ultrasonic lubrication is equally effective in liquid

environments [41], making it suitable for in-vivo applications such as transluminal procedures.

We present a versatile active lubrication sheath that can modulate friction along the shaft of transluminal instruments on demand, building upon

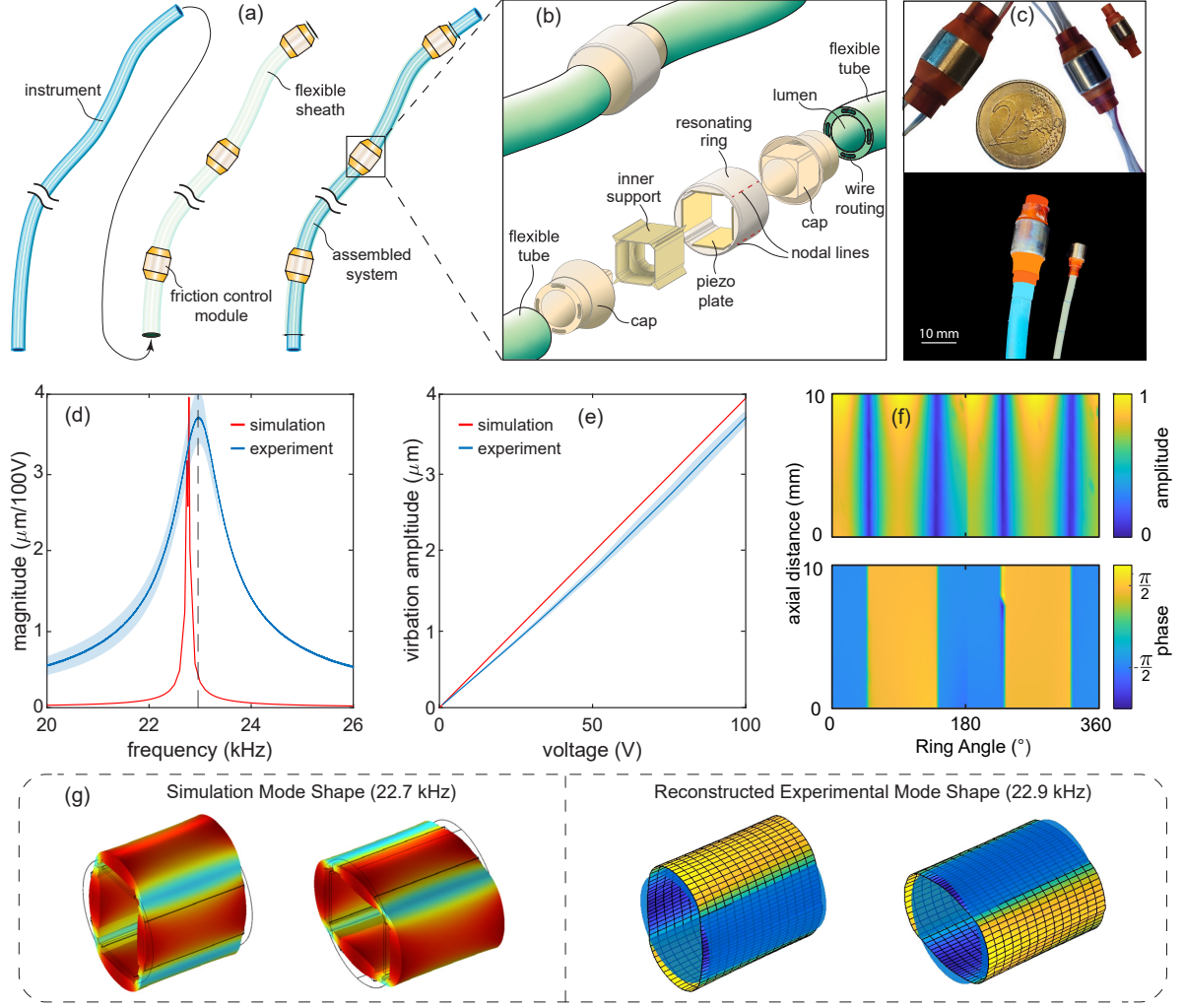


Fig. 2 Design concept and prototype vibration characterization. Each experiment was repeated six times. Solid lines represent the mean of the repetitions and shading represent the standard deviation (a) The proposed active lubrication sheath featuring discrete friction control modules along its shaft. The instrument inserted into this sheath can be actively lubricated on demand. (b) Design of the friction control modules (c) Top: prototypes of 15 mm, 10 mm and 3 mm size. Bottom: fully assembled sheath with friction control module at the tip (d) Frequency response of the resonating ring showing agreement between simulation and experiment. (e) The relationship between amplitude of vibration and input voltage applied to the piezoelectric actuators for simulated and experimental results (f) Mode shape of the resonating ring is the second flexural resonance mode matching simulation (g) comparison between the predicted mode shape by simulation and the experimentally reconstructed mode shape of the resonating ring prototype. (See Supplementary Video 1 for the video demonstration.)

our initial demonstration [42]. This design enables straightforward integration with different transluminal instruments. We show how effective active lubrication modules are at changing friction under varying mechanical loads, surface conditions, and anatomical curvatures. Finally, we validate the system in a cardiac catheterization use case using

ex-vivo porcine aorta tissue, and assess its thermal safety during contact with biological tissues.

Results

Design rationale of active lubrication sheath

The active lubrication sheath features discrete friction control modules distributed along its length, enabling localized, on-demand friction control. When switched on, these modules generate controlled ultrasonic vibrations that induce fluid film lubrication at the module-tissue interface, which transforms the instrument into a low-friction mode for frictionless navigation, as illustrated in Fig. 1(d). Once switched off, the modules re-establish contact with the luminal wall, creating friction-based anchoring for stable execution, as illustrated in Fig. 1(d).

The sheath can function as a catheter or be used to transform existing instruments into actively-lubricated tools by inserting them into the sheath, as illustrated in Fig. 2(a). The modules are slightly larger in diameter than the sheath, to ensure that contact primarily occurs between the modules and the luminal walls, minimizing direct contact between the sheath body and tissue. Additionally, the sheath body is coated with an ultra-low friction material similar to [22] to ensure smooth interaction with the luminal wall, if contact occurs.

Each friction control module generates ultrasonic transverse vibrations through a resonating ring structure equipped with four piezoelectric plates, as shown in Fig. 2(b). When these plates are excited at the resonant frequency of the structure, the latter vibrates along its second flexural resonance mode. The resonance frequency is determined by the diameter of the ring and wall thickness. The resonating ring is supported by an inner support structure made from a self-lubricating material, featuring needle-like edges that hold the ring at the nodal lines of its vibration mode, where the vibration amplitude is near zero. These needle-like supports give way to the nodal lines to rotate freely which minimizes the interference with the vibration. Additionally, the separable support facilitates the assembly of the piezoelectric plates, a crucial feature when miniaturizing the modules.

The resonating rings were specifically engineered to achieve the required resonance mode at an ultrasonic frequency ($> 20 \text{ kHz}$), with vibration amplitudes exceeding ($> 2 \mu\text{m}$), both of which

are key requirements for ultrasonic lubrication to be effective [43, 44]. We developed prototypes in various sizes, ranging from 15 mm to 3 mm, as shown in Fig. 2(c), demonstrating the scalability of the design. To maintain an open lumen, wires are routed through embedded internal channels within the sheath similar to [45], as illustrated in Fig. 2(b). During our characterization and evaluation, we used the 10 mm prototype. Finite element analysis of the 10 mm size ring predicted the resonance frequency to be 22.7 kHz with maximum amplitude in the range of $\approx 4 \mu\text{m}$ per 100 V as shown in Fig. 2(d)(e).

The vibrometry experiments revealed the resonant frequency of the ring structure prototype to be 22.9 kHz and the magnitude to be $\approx 3.7 \mu\text{m}/100\text{V}$, showing close agreement with the simulated frequency response as shown in Fig. 2(d). Moreover, modulating the voltage at the identified resonant frequency reveal the linear relationship between voltage and vibration amplitude, closely matching the simulated model as shown in Fig. 2(e). The laser scanning vibrometry of the surface of the ring excited at the resonant frequency revealed that the mode shape is the second flexural mode as shown in Fig. 2(f)(g). It further revealed that $\approx 84\%$ of the surface of the resonating ring vibrate with sufficient amplitude to induce friction modulation.

Vibration Characterization

Active Lubrication Characterization

To assess how well friction is modulated by the active lubrication module prototypes, we conducted two series of experiments. The first experiment focused on evaluating the performance of the friction control modules under varying conditions, including surface lubricity, applied load, and surface curvature. The second experiment validated the active lubrication efficacy on *ex-vivo* tissue in the transluminal use case of catheters.

In the first set of friction experiments, we used rigid 3D-printed substrates for three main reasons. First, rigid surfaces eliminated the influence of material elasticity, allowing us to isolate the effects of load, surface lubricity, and curvature on friction. Second, rigid substrates are clinically relevant for catheter-based transluminal procedures. While healthy arteries are soft, over 70%

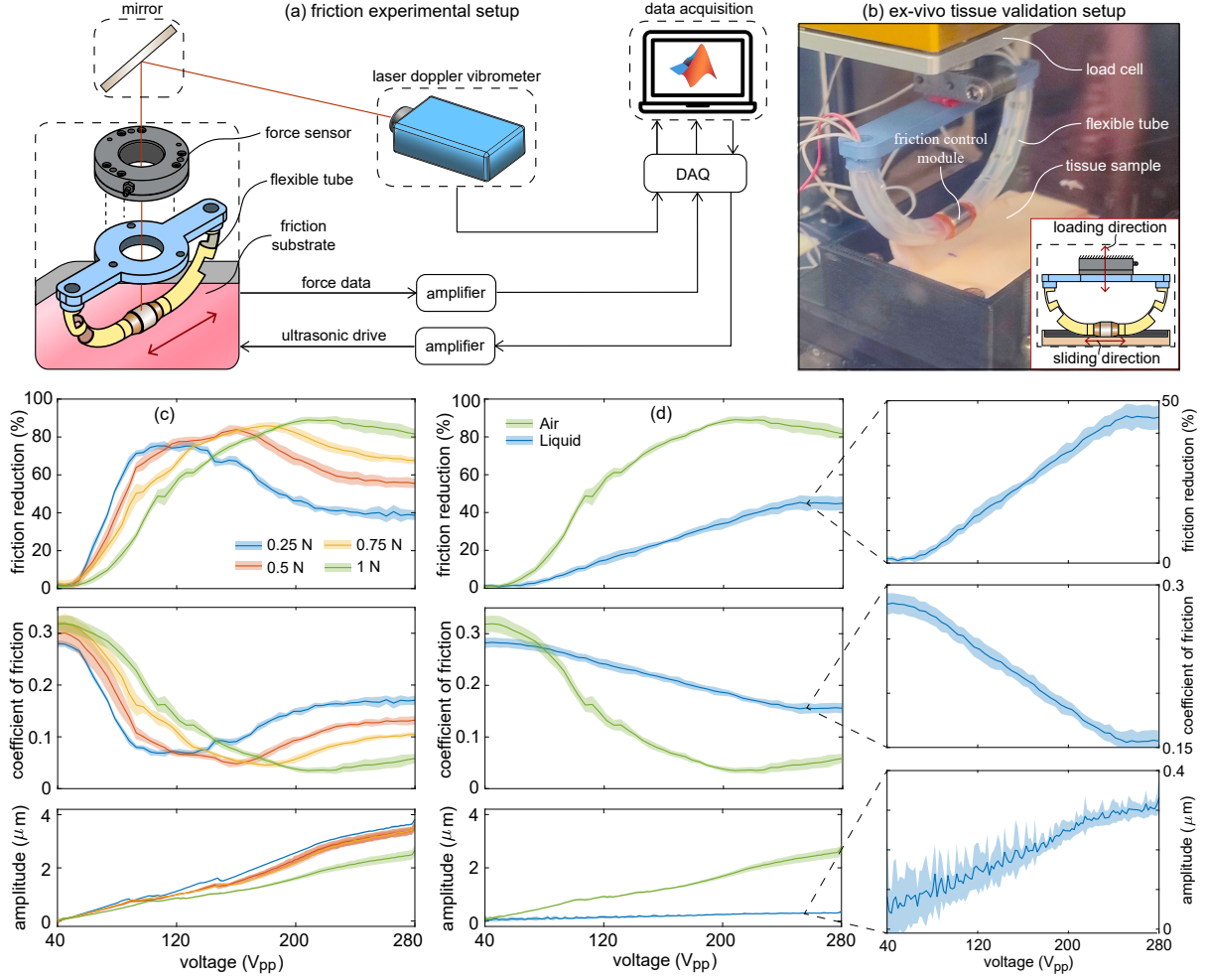


Fig. 3 Characterization of the friction control performance of the active lubrication system. Each experiment was repeated six times. The solid lines represent the mean and shadings represent the standard deviation (a) Experimental setup for friction characterization experiments (b) Experimental setup for ex-vivo tissue validation experiments (c) Shows the friction reduction percentage, coefficient of friction and amplitude as a function of the input voltage at four different loading conditions. We note that the amplitude increases linearly with increasing the input voltage, however, the slope of the amplitude lines decrease as the load increases due to the increased damping. The decrease of friction with amplitude first follow a linear response until $\approx 2 \mu\text{m}$ of amplitude, where it peaks and then decrease slightly. This decrease is likely caused by a saturation in the load carrying capacity of the air squeeze film after, since the added energy is converted into heat leading to a reduction of the levitation force. (d) Shows a comparison between the friction reduction response in air and liquid environment. Unlike air, liquids exhibit a purely linear behavior. The friction reduction for a given amplitude is significantly higher in liquid than in air, suggesting higher load carrying capacity.

of individuals aged 40–49 exhibit some degree of coronary atherosclerosis [46, 47, 48], often resulting in calcified plaque. In patients undergoing catheterization, catheters frequently interact with these rigid, calcified regions, as illustrated in Fig. 1(b). These areas significantly increase friction and can dislodge plaque particles, posing risks as they migrate through the bloodstream

[49]. Third, using rigid surfaces enables direct comparison with state-of-the-art ultrasonic lubrication technologies in the benchmark application of haptic touchscreens [37, 43].

In the second experiment, we used *ex-vivo* tissue samples from a calcification-free porcine aorta, representing the soft elastic end of the arterial mechanical properties. This experiment validated

the effectiveness of the active lubrication system when navigating healthy tissue interfaces in the use case of catheters.

We designed our friction experiments so that contact occurred solely between the active lubrication modules and the friction substrates such that the body of the simulated catheter had no influence, as illustrated in Fig.3(a). The active lubrication modules were supported using flexible tubes to simulate the stiffness-based forces that transluminal instruments exert on tissues, following the configuration in [10], as shown in Fig.3(a). Open-channel substrates, rather than full lumina, offered a real-time vibration tracking during sliding using laser Doppler vibrometry. This measurement directly correlates the amplitude of the ultrasonic vibrations with friction force readings. Similarly, in the *ex-vivo* tissue experiments, the tissue samples were cut open and flattened, as in [50, 10], to ensure controlled friction measurements, as shown in Fig.3(b).

Friction modulation experiment

In this first experiment, we sought to map the relationship between input voltage, vibration amplitude, and friction reduction when in contact with rigid substrates. We also examined how load and lubrication conditions affected both vibration amplitude and friction reduction. To quantify the change in friction when the active lubrication modules were activated, we used the percentage of friction reduction, defined as follows:

$$\text{friction reduction (\%)} = \frac{|\mu_{\text{on}} - \mu_{\text{off}}|}{\mu_{\text{off}}} \quad (1)$$

The friction modulation experiment in dry contact revealed a linear correlation between the amplitude and the input voltage, as shown in Fig.3(c), similar to the contact-free condition in Fig.2(e), albeit with a shallower slope. As the load increases, the slope of the correlation shifts downwards due to the greater damping associated with higher loads. The corresponding friction reduction in all loads first started to increase linearly until it reached a maximum value, followed by a plateau region after which friction reduction gradually declines below its maximum value. We noticed that friction reduction is robust to load, consistently achieving a similar maximum

friction reduction in all loading conditions $\approx 80 - 82\%$, matching the maximum friction reduction achieved by ultrasonic haptic touchscreens [43, 37]. However, increasing the normal load causes a horizontal offset in the friction reduction curve towards higher voltages. This offset is due to the necessity for higher vibration amplitudes to counteract the extra added load, to maintain similar levels of friction reduction. Interestingly, the gradual decline in the friction reduction curve, after its maximum value, occurs despite the corresponding vibration amplitude continuing to increase. We believe that this decline can be attributed to a saturation in the load carrying capacity of the squeeze film in air. That is, the air squeeze film reached its maximum pressure after which increased vibration likely leads to an elevation in the film temperature, causing the air film to become more viscous. As a consequence, more energy is dissipated, reducing the squeeze film pressure and, subsequently, increasing friction.

Friction modulation experiments conducted in liquid-lubricated contact revealed a consistently linear relationship between vibration amplitude and voltage. The amplitude observed was notably smaller, reaching $0.3 \mu\text{m}$ as shown in Fig.3(d), which is seven times less than the amplitude that was observed in air at the maximum input voltage. By examining the corresponding friction reduction, we observe that the reduction of friction begins at around 80 V at which the vibration amplitude becomes sufficient to overcome the interfacial capillary adhesion between the two surfaces. Subsequently, friction reduction follows a linear trend until saturating at a maximum of $\approx 42\%$ friction reduction as shown in Fig.3(d), approximately twice as smaller than its air counterpart. The higher friction reduction to vibration amplitude ratio in the liquid case underscores the greater load carrying capacity of liquid films, in alignment with the incompressible squeeze-film levitation theory [41]. We also observe that liquid-lubricated contact exhibits a linear behavior for a wider range of input voltage in comparison to air. Moreover, saturation of the reduction of friction is caused by a saturation of the vibration amplitude, unlike in the dry condition where the saturation comes from the load carrying capacity of the air film. This indicates that the saturation of the friction reduction is not due to a limit in the liquid load-carrying capacity, but rather the ability to

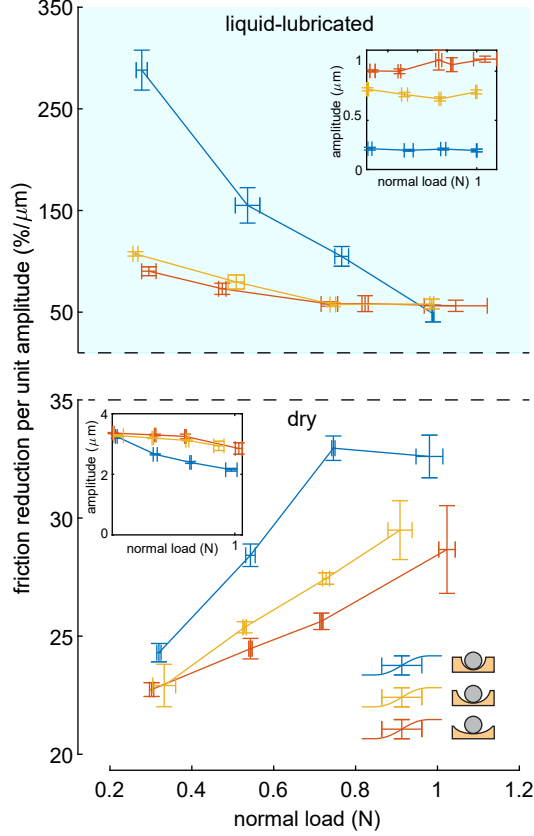


Fig. 4 Effect of surface curvature on the performance of the active lubrication modules in dry and lubricated contact conditions at different loads. Each condition was repeated six times, with points representing the mean and the error bars representing the standard deviation. In the dry condition at constant load, the friction reduction capacity (friction reduction per unit amplitude) increases with the curvature of the surface which can be attributed to the corresponding increase in contact area. The inset shows that the vibration amplitude decreases as the load increases due to the associated increased damping. In the liquid-lubricated contact, we observe that the friction reduction capacity is significantly greater than its dry counterpart which is due to the significantly higher load carrying capacity of liquid squeeze films as explained by the incompressible squeeze-film theory [41]. We observe that the most curved surface exhibits significantly higher friction reduction capacity at lower loads, which decreases afterwards due to the increased resistance for the liquid to squeeze in and out of the film area, resulting in increased energy dissipation that lowers the friction reduction capacity overall. The inset shows a nearly constant vibration amplitude across all loads which is likely due to the module vibrating on top of the fully-developed squeeze film.

produce sufficient amplitude in a high dissipation environment.

Surface curvature experiment

To assess the effect of surface curvature, we performed friction experiments on substrates with different diameter ratios, which is the ratio of the module diameter to the substrate diameter. Our study examined three diameter ratios: 0.37, 0.67, and 0.98, representing surfaces that transition from almost flat to highly curved. The results further demonstrated that liquid-lubricated contact is superior to dry contact in friction modulation capacity. This capacity is the friction reduction percentage per unit vibration amplitude as shown in Fig.4. This superiority implies that at the same load and vibration amplitude, liquid-lubricated contact can achieve greater friction reduction compared to dry contact.

In dry contact conditions, we observed that the vibration amplitude decreases with increasing load in all three curvature profiles, as shown in the inset of Fig.4. This can be attributed to an increase in viscous losses caused by higher loads. Additionally, at a given load, the vibration amplitude decreases with increasing diameter ratio, which can be attributed to the larger contact area and the resulting increase in damping. For the friction reduction capacity, we found that at the same load, surfaces with higher curvature exhibited greater friction reduction capacity, which can be explained by the greater contact area generating a proportional increase in the squeeze film force [41], as shown in Fig.4. Moreover, the friction reduction capacity improved with increasing load across all curvature profiles. This trend is likely due to the reduced interfacial gap thickness between the two surfaces at higher loads, enhancing the squeeze film force, which results in greater friction reduction at the same vibration amplitude.

Looking at the liquid-lubricated contact in Fig.4, we notice that the vibration amplitude, shown in the inset, remains almost constant across all loads. This constancy is likely due to the vibrating module being levitated and vibrating on top of a liquid squeeze film. In addition, the friction reduction capacity is reduced as the load increases, most likely because at higher loads, the interfacial gap thickness between the two surfaces becomes smaller, which in turn impedes the liquid from flowing in and out of the interface.

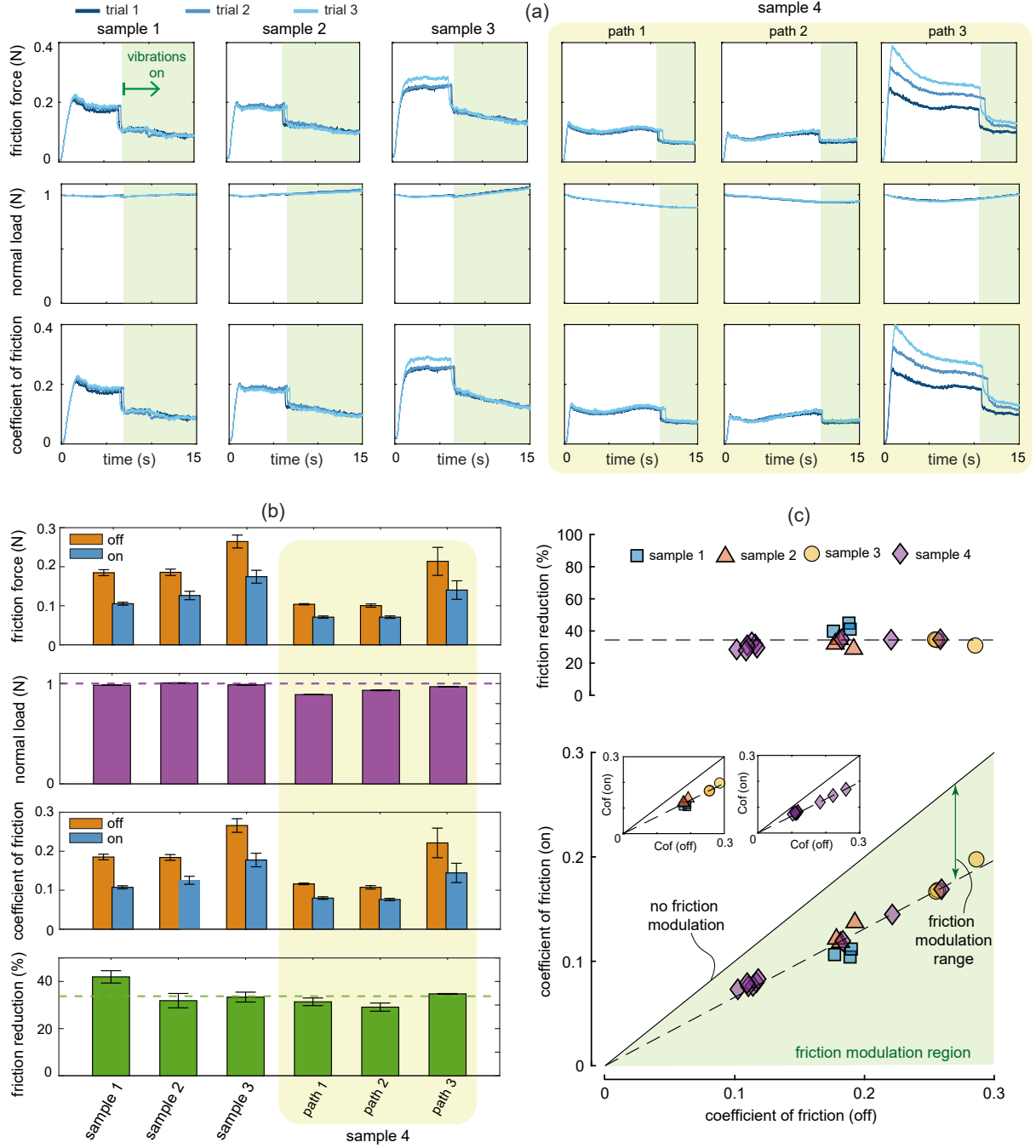


Fig. 5 Friction validation experiments on *ex-vivo* porcine aorta tissue. Each experiment was repeated six times. The first three repetitions were used for preconditioning the tissue, while the last three were used for analysis. (a) Recorded friction, normal load and coefficient of friction data across different samples and paths. The data shows that upon activating vibrations, the friction force drops immediately, demonstrating the active lubrication principle. (b) Comparison of the different samples and paths, with the bars representing the mean and the error bars representing the standard deviation. The friction force and coefficient of friction vary across all tissue samples and paths. This effect is partly due to the topography of the tissue sample that causes uneven distribution of the lubrication liquid. The testing samples dried out over time which caused the a slight increase coefficient of friction for later trials. The spatial variance in normal load is mainly due to the topography of the tissue samples. (c) Linear correlation between the coefficient of friction in the off condition μ_{off} (before enabling vibrations) and the coefficient of friction in the on condition μ_{on} (after enabling vibrations).

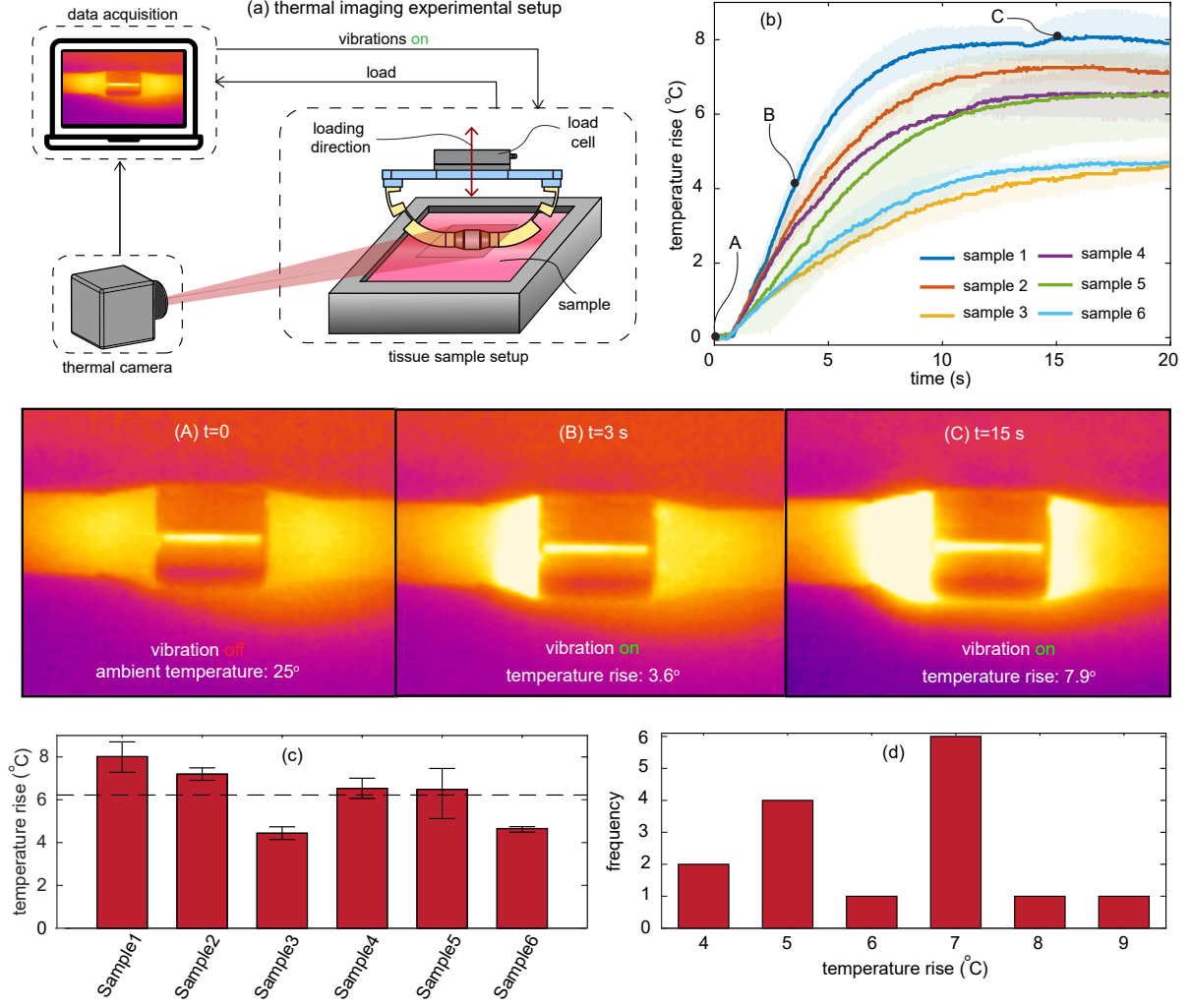


Fig. 6 Thermal imaging of active lubrication modules during operation. Each experiment was repeated three times. The solid lines and bars represent the mean while the shadings and error bars represent the standard deviation (a) Experimental setup comprising a thermal camera recording the thermal footprint of the active lubrication modules when loaded against dry tissue samples in ambient room temperature. (b) Time response of the temperature of the friction control modules. Upon activation, the temperature rises until it reaches a steady state temperature after 10 seconds of activation. (c) Recorded temperature rise across six tissue samples averaging at 6.2°C , with error bars representing the standard deviation. (d) Histogram of the recorded temperature rise, revealing 7°C to be the most frequently observed temperature rise, which is within the safety limit [51, 52]. (See Supplementary Video 2 for the video demonstration.)

This free movement of the liquid is a crucial factor for squeeze film pressure to develop in liquid films [41]. We observe that the most curved interface in the liquid-lubricated case initially exhibits significantly larger friction reduction capacity as compared to the other two profiles. It can be explained by the larger surface area contributing to an increased squeeze film force. However, the friction reduction capacity rapidly declines as the

load increases due to the higher resistance for the liquid to move across the film. This larger resistance causes the liquid to lose more energy and thus reduces its load-carrying capacity.

Based on the linear correlation, between friction and the vibration amplitude, we observed in the friction modulation experiment Fig.3(d),

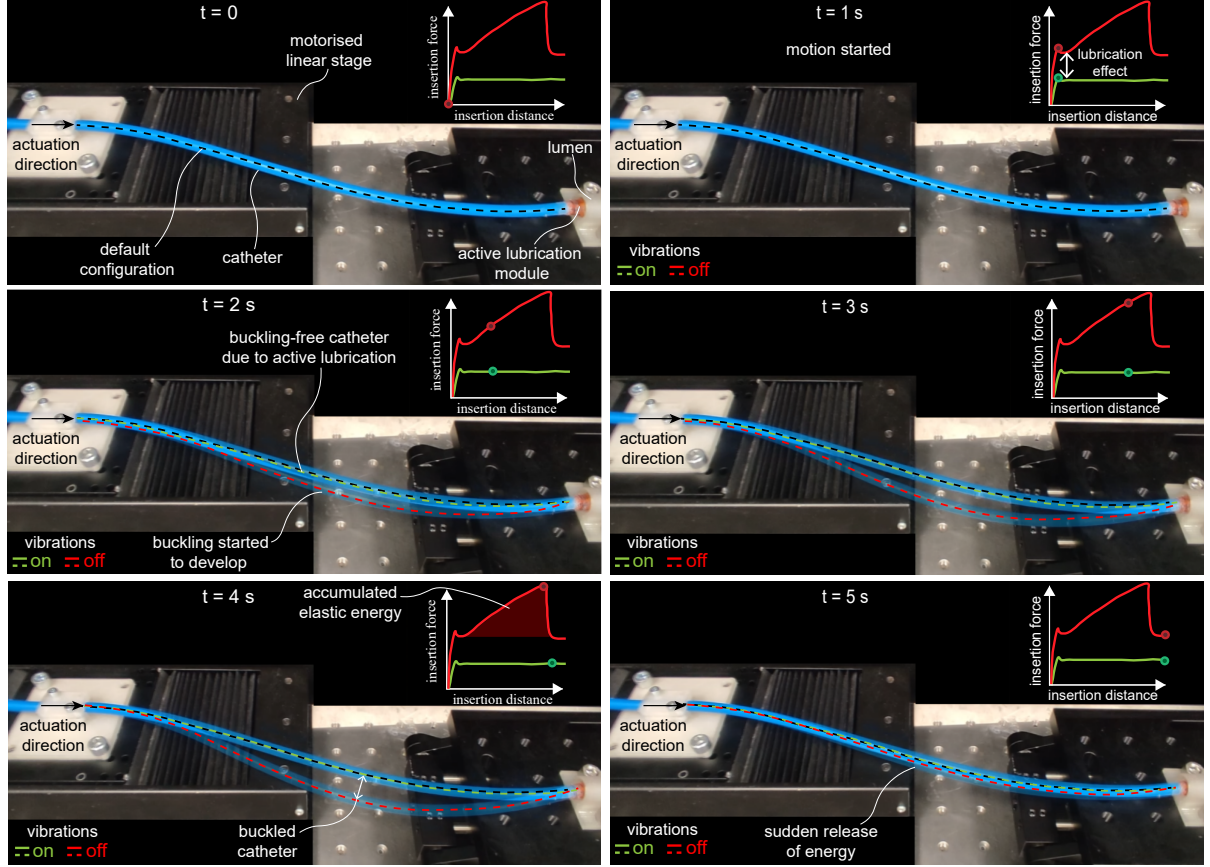


Fig. 7 Demonstration of the effect of active lubrication in preventing buckling of catheters during insertion. We integrated an active lubrication catheter, with a friction control module at the tip, into a 3D printed lumen, both with and without activating lubrication. The catheter actuation base was deliberately misaligned with respect to the lumen, increasing frictional interaction with the wall and thus simulating real-world conditions. Without active lubrication, the catheter tip experienced higher friction, causing it to buckle. This buckling accumulated elastic energy in the shaft of the catheter until the energy was suddenly released. This release rapidly moved forward the catheter, potentially exerting excessive shock load on the lumen wall. In contrast, with the active lubrication system activated, the catheter tip moved smoothly through the lumen without buckling maintaining low frictional interaction with the luminal wall. (See Supplementary Video 3 for the video demonstration.)

one can assume that the behavior in the liquid-lubricated case, shown in Fig. 4 holds across different input voltages. However, for dry contact, the same conclusion may only be applied in the linear region of the the response in Fig. 3(c), while the other region is likely voltage-dependent.

We conclude that highly curved surfaces are more favorable for friction reduction in both dry and liquid-lubricated environments. This conclusion is supported by the fact that friction force does not depend on the apparent area of contact. As curvature increases, the apparent area of contact increases, enhancing the squeeze-film force

without affecting the friction force, resulting in a net increase in the friction reduction capacity.

***Ex-vivo* tissue validation**

We validated our active lubrication catheter on liquid-lubricated *ex-vivo* porcine aorta tissues, simulating a representative cardiac catheterization scenario. We tested our design on four different samples. In addition, we evaluated the active lubrication performance along three different paths on the same sample to determine if it was path-dependent. We hydrated the surface of each sample with phosphate buffered saline (PBS)

solution, and conducted six trials for each experiment. The first three trials were primarily used for conditioning the tissues, thus only the final three trials were considered in the analysis. Experiments were conducted under a load of 1 N , a critical load for catheters [53]. Upon enabling vibrations, the coefficient of friction dropped immediately to a lower level as shown in Fig.5(a), with friction reduction up to 42% and an average of 38% across all tissue samples and paths at maximum vibration amplitude as shown in Fig.5(b).

Looking closely at the results in Fig.5(a)&(b), we first observe fluctuations of the normal load across the different samples and paths with small variance across trials. These fluctuations result from the non-uniform topography of the tissue samples along the sliding path. Second, we observe that the starting coefficient of friction (before vibrations are activated) μ_{off} varied between samples, paths and between trials (example in Fig.5(a) - Sample 4-Path 3). This variation across samples and paths can be attributed to the uneven surface topography of tissue samples which resulted in uneven distribution of the surface lubrication layer. In addition, we observed that the tissue samples were drying out over time, resulting in increasing friction levels across the different trials.

This seemingly undesired variance in the coefficient of friction revealed an interesting correlation between the coefficient of friction in the off condition (before vibrations are activated) μ_{off} and the coefficient of friction in the on condition (after vibrations are activated) μ_{on} as shown in Fig. 5(c). The coefficient of friction in the on condition μ_{on} is positively correlated to the coefficient of friction in the off condition μ_{off} and this correlation holds for both different samples and different paths as shown in the insets of Fig.5(c). This correlation is well explained by the model of Wiertlewski et al. [36] in which they showed using multi-scale contact theory [54, 55, 56] and the squeeze film theory [57, 35] that the coefficient of friction after enabling vibrations μ_{on} is proportional to the coefficient of friction without vibrations μ_{off} as follows:

$$\mu_{\text{on}} = \beta \cdot \mu_{\text{off}} \cdot \exp\left(\frac{\alpha}{N}\right) \quad (2)$$

where α is the vibration amplitude, N is the normal load and β is a proportionality constant that depends on surface roughness and material elasticity. This equation implies that the slope

of the friction modulation line depends on the vibration amplitude and normal load. At identical vibration amplitude and load, the range between μ_{off} and μ_{on} , as shown in Fig.5(c), increases linearly with the increase in μ_{off} , while the friction reduction percentage (%) remains constant.

This correlation between the coefficient of friction in on (μ_{on}) and off (μ_{off}) conditions, shown in Fig.5(c), provides key design insights for optimizing the active lubrication system. Specifically, it is beneficial to maximize both the starting coefficient of friction (μ_{off}) and the vibration amplitude. Higher μ_{off} increases the difference between μ_{off} and μ_{on} at maximum vibration amplitude, enabling more effective switching between friction states. Similarly, maximizing vibration amplitude increases the controllable range between μ_{off} and μ_{on} for a given starting coefficient of friction μ_{off} . Combining both factors can potentially result in a wider controllable range, with higher friction in the "off" state and lower friction in the "on" state. However, further investigation is needed to determine the optimal controllable range and the acceptable limits for interacting with tissues. That is to find the most effective range of vibration which switches between friction states that minimizes tissue damage while ensuring stability during catheterization.

Thermal imaging experiment

Excessive heat from vibration can pose serious risks, as it may lead to significant tissue damage, including tissue necrosis [58]. It is therefore important to investigate this risk, we conducted an experiment monitoring the heat produced at the interface between the active lubrication modules and tissue samples using a thermal camera, as shown in Fig.6(a). We performed an indentation test in which active lubrication modules were pushed onto tissue samples with a normal load of 1 N . Vibrations were then activated without any sliding and under surface-lubricated condition, while measuring the temperature rise at ambient room temperature 20 – 22°C. We observed that the temperature at the module-tissue interface started to rise as soon as vibrations are activated until it reached a steady state temperature after approximately ten seconds, as shown in Fig.6(b). We found the average temperature rise to be $\approx 6.2^\circ C$, as shown in Fig.6(c), with

7° C being the most frequent temperature rise as shown in Fig.6(d). This temperature rise translates to $\approx 44^\circ \text{C}$ inside the human body which is within the thermal safety range for the human body [51, 52], suggesting the potential thermal safety of this technology for transluminal surgery applications.

It is important to note that the thermal safety tests were conducted in a dry, ambient room temperature environment without sliding and the real-life results would most likely differ since the system will be placed inside a blood vessel. First, the temperature rise observed at room temperature may not necessarily reflect what occurs at nominal body temperature. Second, conducting the experiment in dry condition likely underestimated the cooling effect that blood flow would have. Blood flow would naturally dissipate heat through convection, reducing overall heat accumulation in the modules. Lastly, the temperature increase is localized at the module-tissue interface, and since this interface constantly changes position during catheter navigation, tissue exposure to heat would be limited in time, further supporting thermal safety. While these findings offer promising insights into heat generation for ultrasonically-lubricated catheters, more rigorous testing in clinically relevant environments is needed to fully assess heat generation and its potential effects on tissue.

Catheter buckling experiment

To demonstrate the impact of the active lubrication technology, we conducted an experiment where we inserted a catheter with an integrated active lubrication module at its tip into a 3D printed lumen, both with and without ultrasonic lubrication activation. The catheter base was deliberately misaligned with respect to the lumen, to induce frictional interaction with the wall, simulating real-world conditions. As shown in Fig.7, without lubrication, the catheter tip experienced higher friction, causing the catheter to buckle. This buckling resulted in elastic energy accumulation in the shaft of the catheter until it was suddenly released; rapidly advancing the catheter tip forward. This sudden release of energy can exert excessive forces on the luminal wall, potentially causing catastrophic lumen dissection or

rupture [21, 22]. In contrast, with the lubrication module activated, the catheter tip moved smoothly through the lumen without buckling, as seen in Fig.7, maintaining low frictional interaction with the lumen wall. This demonstration underscores the positive impact of the active lubrication system in reducing catheter buckling, potentially enhancing insertion and navigation, and thus ultimately improving the safety and efficacy of transluminal procedures.

Discussion

We introduced an active lubrication catheter that can modulate friction on demand, enabling smoother and complication-free transluminal procedures. The catheter uses active lubrication modules that produce ultrasonic micrometer-range transverse vibrations to create a fluid film lubrication. This lubrication facilitates frictionless navigation and stable precise execution of surgical tasks. We presented a scalable design for the lubrication modules, accommodating the varying size requirements of transluminal instruments. Vibrometry experiments demonstrated that the modules achieved displacements of 3.7 μm at 100 V at an ultrasonic frequency of 22.7 kHz, with the active lubrication surface covering approximately 85% of the total module area.

In tribometric experiments, we showed that the modules can control friction in both dry and liquid-lubricated conditions, across rigid and *ex-vivo* tissue interfaces. In these experiments, friction was reduced by up to 42% on *ex-vivo* tissue and by up to 82% on rigid surfaces, respectively representing healthy and calcified tissue in the example of cardiac catheterization application. The *ex-vivo* tissue experiments demonstrated how ultrasonic lubrication can be a powerful tool to modulate friction on liquid-lubricated tissue interfaces in real-time. These experiments also revealed a key correlation between the "off" (μ_{off}) and "on" (μ_{on}) friction states. To expand the controllable friction modulation range both the initial coefficient of friction and vibration amplitude needs to be increased. Additionally, it is clear that the active lubrication works at its best in liquid-lubricated environments. Similarly, higher curvature interfaces are more favorable for active lubrication, possibly due to its larger contact area. Despite intense vibrations, the temperature rise

was on average 6.2°C , which is well within safe limits for tissue thermal safety [51, 52]. Finally, during insertion, the active lubrication showed a drastic reduction of the probability of buckling. The reduced friction, due to active lubrication, with the lumen wall allowed a smooth insertion of the catheter.

In future work, we aim to extend validation to a range of tissue types, including intestinal tissue, to assess its applicability across different transluminal applications. Additionally, we plan to conduct histological examinations on tissue samples to systematically study the effects of vibrations and determine if the active-lubrication modules induce any potential damage. We will also optimize the configuration of the active lubrication modules, focusing on their spacing and their ideal sizes. Finding the optimal form factor can also drastically improve the effectiveness of the modules. We plan to develop a waterproof design to facilitate testing in fully submerged liquid environments, which is particularly important for catheter applications. With the waterproofing, we will be able to conduct in-vivo animal studies with fully assembled instruments, bringing our testing closer to clinical settings.

While this study focused on cardiovascular applications, the findings can be extended to other field of applications. The technology can be applied to procedures involving catheters and endoscopic devices, where active lubrication is equally crucial. Our characterization of the system under varying conditions of load, surface lubricity, and curvature provides a solid foundation for its broader applicability across diverse medical scenarios. These results establish a baseline for the technology performance in different environments and can inspire future advancements, ultimately benefiting a wide range of transluminal procedures.

Methods

Vibration characterization experiment

In this experiment, we characterized the vibration response of the resonating ring to varying voltage inputs using a single-point laser Doppler vibrometer (LDV) (OFV5000, Polytec GmbH, Baden-Württemberg, Germany). To achieve a full surface scan of the ring, the ring was mounted on a servo

motor, allowing it to rotate. This enabled scanning at various orientations while the LDV's laser beam was directed via a dual-axis galvanometer (ScannerMAX Saturn 5B, Edmund Optics Inc., NJ, USA), based on a scanning setup similar to the one in [42]. The galvanometer facilitated longitudinal scans, while the servo motor adjusted the orientation of the resonating ring. A MATLAB interface managed the operation of the galvanometer, servo motor, and LDV, coordinating the data acquisition process through National Instruments data acquisition card (USB-6356, National Instruments, TX, USA).

For performance evaluation, we focused on four key parameters: resonant frequency, peak vibration amplitude, vibration mode, and the effective surface area. The effective area is defined as the region where vibration amplitudes equal or exceed two microns, aligning with the technological specifications. To gather these data, we conducted three types of measurements: a frequency response analysis to determine the resonant frequency, a voltage sweep at that frequency to measure the maximum amplitude, and a surface scan of the ring to assess the vibration mode and calculate the effective area.

The experiment began by performing a frequency sweep at the center of each of the four anti-nodal lines, followed by a voltage sweep at the identified resonant frequency. Surface scanning then commenced with the ring positioned at an anti-nodal line aligned with the laser beam. The measurable path was divided into ten discrete points along the length of the ring. The transducers were activated to record data at each point. After scanning one line, the ring was rotated by 5 degrees, and this process repeated until the entire surface of the ring was covered, producing a comprehensive dataset.

Friction characterization experiment

In this experiment, we mounted the ring structure to a 6-axis force sensor (Nano43, ATI Industrial Automation, NC, U.S.A.). The module-sensor assembly was affixed to a manual linear slider to regulate the normal load. The friction substrates, affixed opposite to the surface of the resonating ring, were allowed to slide against the ring surface using a motorized linear stage. Simultaneously, the

LDV measured the vibration amplitude from top of the resonating ring while sliding.

The experimental protocol began with loading the resonating ring onto the friction substrate to (1 N). Then, the substrate started to slide at 1 mm/s for a distance of 15 mm. Two set of experimental data were collected. First, we activated a linearly modulated input voltage amplitude from a minimum to a maximum voltage for a period of five seconds while sliding, and we recorded the corresponding friction and vibration amplitude. We conducted this experiment in different loading and surface lubricity conditions. Each sliding friction test was repeated six times. Second, we conducted experiments on surfaces with different curvatures. In this experiment, the friction control modules were activated five seconds after sliding started at maximum input voltage. Then, the recorded amount of friction reduction was normalized by the recorded vibration amplitude to get the friction reduction capacity. Experiment was conducted in different loading conditions and each condition was repeated six times.

***ex-vivo* tissue validation experiment**

Porcine aorta (approximately 6 months old) were obtained within 2 hours of slaughter directly from a local abattoir. The aorta were preserved in 4 °C phosphate-buffered saline (PBS) solution after being cut and transported in an insulated container to maintain their hydration and integrity. Samples were cut and gently washed with PBS to remove residues without damaging the tissue layer. Rectangular sections, 10 mm in length were excised along the axis of the artery. Then, tissues were stored at −80 °C for up to 30 days to retain the original condition as much as possible. The tissue was fully thawed before testing, and hydration was maintained with PBS during the experiments.

Sliding friction experiments were conducted on four tissue samples, with each experiment repeated six times along the same path. To assess path-dependence, we also evaluated the active lubrication performance along three distinct paths on the same sample. The first three trials of each experiment were used to condition the tissue; therefore, only the final three repetitions were included in the analysis.

Thermal imaging experiment

In this experiment, a thermal camera (thermoIM-AGER TIM 160S, Micro-Epsilon, NC, USA) was used to capture the temperature rise at the interface between the active lubrication modules and ex vivo tissue samples. The experimental protocol began with hydrating the tissue surface using phosphate-buffered saline (PBS), followed by applying a normal load of 1 N to the active lubrication modules. Once loaded, the modules were activated, and the temperature increase at the interface was continuously monitored. Experiments were performed on six different tissue samples, with each experiment repeated three times.

Acknowledgments. This work was funded by a Delft University of Technology cohesion grant. The experimental work was supported by a EPSRC (UK) Centre-to-Centre Grant “Tribology as an Enabling Technology (TRENT)” (EP/S030476/1).

Data Availability. All relevant data are available from the corresponding authors upon request.

References

- [1] M. S. Wagh and C. C. Thompson, “Surgery insight: natural orifice transluminal endoscopic surgery—an analysis of work to date,” *Nature Clinical Practice Gastroenterology & Hepatology*, vol. 4, no. 7, pp. 386–392, 2007.
- [2] O. M. Omisore, S. Han, J. Xiong, H. Li, Z. Li, and L. Wang, “A Review on Flexible Robotic Systems for Minimally Invasive Surgery,” *IEEE Transactions on Systems, Man, and Cybernetics: Systems*, vol. 52, no. 1, pp. 631–644, 2022.
- [3] M. Runciman, A. Darzi, and G. P. Mylonas, “Soft robotics in minimally invasive surgery,” *Soft Robotics*, vol. 6, no. 4, pp. 423–443, 2019. PMID: 30920355.
- [4] R. M. Wagner, R. Maiti, M. J. Carré, C. M. Perrault, P. C. Evans, and R. Lewis, “Biotribology of Vascular Devices: A Review of Tissue/Device Friction Research,” *Biotribology*, vol. 25, no. October 2020, 2021.
- [5] X. Zhang, Y. Zhang, and Z. Jin, “A review of the bio-tribology of medical devices,” *Fric-tion*, vol. 10, no. 1, pp. 4–30, 2022.

- [6] K. H. Dellimore, A. R. Helyer, and S. E. Franklin, "A scoping review of important urinary catheter induced complications," *Journal of Materials Science: Materials in Medicine*, vol. 24, no. 8, pp. 1825–1835, 2013.
- [7] K. H. Dellimore, S. E. Franklin, and A. R. Helyer, "A Review of Catheter Related Complications During Minimally Invasive Transcatheter Cardiovascular Intervention with Implications for Catheter Design," *Cardiovascular Engineering and Technology*, vol. 5, no. 3, pp. 217–232, 2014.
- [8] K. H. Dellimore, A. J. Mank, J. Wojnowski, C. Noble, and S. E. Franklin, "Evaluation of catheter-induced tribological damage to porcine aorta using infra-red spectroscopy," *Biotribology*, vol. 7, pp. 11–21, 2016.
- [9] L. E. Bostan, C. Noble, N. Smulders, R. Lewis, M. J. Carré, S. Franklin, N. H. Green, and S. MacNeil, "Measurement of Friction-induced Changes in Pig Aorta Fibre Organization by Non-invasive Imaging as a Model for Detecting the Tissue Response to Endovascular Catheters," *Biotribology*, vol. 12, no. May, pp. 24–32, 2017.
- [10] C. Lin, H. J. Kaper, W. Li, R. Splinter, and P. K. Sharma, "Role of endothelial glycocalyx in sliding friction at the catheter-blood vessel interface," *Scientific Reports*, vol. 10, no. 1, p. 11855, 2020.
- [11] Z. Wang, K. Wang, and Y. Xu, "Friction injury of the central vein caused by catheter for hemodialysis: an in vitro study," *Scientific Reports*, vol. 14, no. 1, p. 5836, 2024.
- [12] W. Li, L. Shi, H. Deng, and Z. Zhou, "Investigation on friction trauma of small intestine in vivo under reciprocal sliding conditions," *Tribology Letters*, vol. 55, no. 2, pp. 261–270, 2014.
- [13] W. Waddingham, U. Kamran, B. Kumar, N. J. Trudgill, Z. P. Tsiamoulos, and M. Banks, "Complications of diagnostic upper Gastrointestinal endoscopy: common and rare – recognition, assessment and management," *BMJ Open Gastroenterology*, vol. 9, no. 1, p. e000688, 2022.
- [14] S. Y. Kim, H. S. Kim, and H. J. Park, "Adverse events related to colonoscopy: Global trends and future challenges," *World Journal of Gastroenterology*, vol. 25, no. 2, pp. 190–204, 2019.
- [15] C. X. Lin, Q. Y. Yu, J. Wang, W. Ji, W. Li, and Z. R. Zhou, "Friction behavior between endoscopy and esophageal internal surface," *Wear*, vol. 376–377, pp. 272–280, 2017.
- [16] C. Lin, W. Li, H. Deng, K. Li, and Z. Zhou, "Friction behavior of esophageal mucosa under axial and circumferential extension," *Tribology Letters*, vol. 67, pp. 1–14, 2019.
- [17] C. Lin, W. Liu, J. Xie, W. Li, and Z. Zhou, "The lubricating function of mucin at the gastroscope device-esophagus interface," *Tribology Letters*, vol. 68, pp. 1–10, 2020.
- [18] J. O. Perreault and C. G. Cao, "Effects of vision and friction on haptic perception," *Human Factors*, vol. 48, no. 3, pp. 574–586, 2006.
- [19] A. M. Okamura, L. N. Verner, C. E. Reiley, and M. Mahvash, "Haptics for robot-assisted minimally invasive surgery," *Springer Tracts in Advanced Robotics*, vol. 66, no. STAR, pp. 361–372, 2010.
- [20] E. P. van der Putten, R. H. Goossens, J. J. Jakimowicz, and J. Dankelman, "Haptics in minimally invasive surgery - A review," *Minimally Invasive Therapy and Allied Technologies*, vol. 17, no. 1, pp. 3–16, 2008.
- [21] T. Gopesh, J. H. Wen, D. Santiago-Dieppa, B. Yan, J. S. Pannell, A. Khalessi, A. Norbash, and J. Friend, "Soft robotic steerable microcatheter for the endovascular treatment of cerebral disorders," *Science Robotics*, vol. 6, no. 57, p. eabf0601, 2021.
- [22] L. Mao, P. Yang, C. Tian, X. Shen, F. Wang, H. Zhang, X. Meng, and H. Xie, "Magnetic steering continuum robot for transluminal procedures with programmable shape and functionalities," *Nature Communications*, vol. 15, no. 1, p. 3759, 2024.
- [23] A. Sakes, D. Dodou, and P. Breedveld, "Buckling prevention strategies in nature as inspiration for improving percutaneous instruments: A review," *Bioinspiration and Biomimetics*, vol. 11, no. 2, 2016.
- [24] H. Baek, B. Cheon, J. M. You, and D. S. Kwon, "Design and analysis of feeder mechanism for buckling prevention in robotic catheterization," *Journal of Computational Design and Engineering*, vol. 9, no. 4, pp. 1467–1481, 2022.
- [25] Y. Muranishi, T. Sato, Y. Ueda, Y. Yutaka,

- T. Nakamura, and H. Date, "A novel suction-based lung-stabilizing device in single-port video-assisted thoracoscopic surgical procedures," *General Thoracic and Cardiovascular Surgery*, vol. 68, no. 5, pp. 503–507, 2020.
- [26] A. Loeve, P. Breedveld, and J. Dankelman, "Scopes too flexible and too stiff," *IEEE Pulse*, vol. 1, no. 3, pp. 26–41, 2010.
- [27] T. Ranzani, S. Russo, F. Schwab, C. J. Walsh, and R. J. Wood, "Deployable stabilization mechanisms for endoscopic procedures," *Proceedings - IEEE International Conference on Robotics and Automation*, pp. 1125–1131, 2017.
- [28] E. Brocchi, R. Pezzilli, P. Tomassetti, D. Campana, A. M. Morselli-Labate, and R. Corinaldesi, "Warm water or oil-assisted colonoscopy: Toward simpler examinations?," *American Journal of Gastroenterology*, vol. 103, no. 3, pp. 581–587, 2008.
- [29] M. Wilson, "Catheter lubrication and fixation: interventions," *British Journal of Nursing*, vol. 22, no. 10, pp. 566–569, 2013.
- [30] A. Hernandez, R. Cogdill, C. Hinojosa-Laborde, and M. I. Restrepo, "Comparison of silicone spray versus water soluble lubricating jelly for the aid in bronchoscopic examination," *Journal of Anesthesiology and Clinical Science*, vol. 2, no. 1, p. 7, 2013.
- [31] J. Wang, L. Ma, W. Li, and Z. Zhou, "Influence of different lubricating fluids on friction trauma of small intestine during enteroscopy," *Tribology International*, vol. 126, no. February, pp. 29–38, 2018.
- [32] N. Watanabe, R. Hirose, H. Ikegaya, K. Yamauchi, H. Miyazaki, T. Yoshida, R. Bandou, K. Inoue, O. Dohi, N. Yoshida, *et al.*, "Identification of lubricant viscosity to minimize the frictional impact of colonoscopy on colonic mucosa," *Communications Engineering*, vol. 3, no. 1, p. 31, 2024.
- [33] P. Wyman, "Hydrophilic coatings for biomedical applications in and ex vivo," *Coatings for Biomedical Applications*, pp. 3–42, 2012.
- [34] A. Niemczyk, M. El Fray, and S. E. Franklin, "Friction behaviour of hydrophilic lubricious coatings for medical device applications," *Tribology International*, vol. 89, pp. 54–61, 2015.
- [35] E. O. J. Salbu, "Compressible Squeeze Films and Squeeze Bearings," *Journal of Basic Engineering*, vol. 86, pp. 355–364, 06 1964.
- [36] M. Wiertelowski, R. F. Friesen, and J. E. Colgate, "Partial squeeze film levitation modulates fingertip friction," *Proceedings of the National Academy of Sciences of the United States of America*, vol. 113, no. 33, pp. 9210–9215, 2016.
- [37] L. Winfield, J. Glassmire, J. E. Colgate, and M. Peshkin, "T-PaD: Tactile pattern display through variable friction reduction," *Proceedings - Second Joint EuroHaptics Conference and Symposium on Haptic Interfaces for Virtual Environment and Teleoperator Systems, World Haptics 2007*, pp. 421–426, 2007.
- [38] R. Gabai, R. Shaham, S. Davis, N. Cohen, and I. Bucher, "A Contactless Stage Based on Near-Field Acoustic Levitation for Object Handling and Positioning-Concept, Design, Modeling, and Experiments," *IEEE/ASME Transactions on Mechatronics*, vol. 24, no. 5, pp. 1954–1963, 2019.
- [39] S. Zhao, S. Mojrzisch, and J. Wallaschek, "An ultrasonic levitation journal bearing able to control spindle center position," *Mechanical Systems and Signal Processing*, vol. 36, no. 1, pp. 168–181, 2013.
- [40] M. Shi, K. Feng, J. Hu, J. Zhu, and H. Cui, "Near-field acoustic levitation and applications to bearings: A critical review," *International Journal of Extreme Manufacturing*, vol. 1, no. 3, 2019.
- [41] M. A. Atalla, R. A. J. van Ostayen, A. Sakes, and M. Wiertelowski, "Incompressible squeeze-film levitation," *Applied Physics Letters*, vol. 122, no. 24, 2023.
- [42] M. A. Atalla, J. J. Tuijp, M. Wiertelowski, and A. Sakes, "Toward variable-friction catheters using ultrasonic lubrication," *IEEE Transactions on Medical Robotics and Bionics*, pp. 1–1, 2024.
- [43] M. Biet, F. Giraud, and B. Lemaire-Semail, "Squeeze film effect for the design of an ultrasonic tactile plate," *IEEE Transactions on Ultrasonics, Ferroelectrics, and Frequency Control*, vol. 54, no. 12, pp. 2678–2688, 2007.
- [44] T. Watanabe and S. Fukui, "A method for

- controlling tactile sensation of surface roughness using ultrasonic vibration,” in *Proceedings of 1995 IEEE International Conference on Robotics and Automation*, vol. 1, pp. 1134–1139 vol.1, 1995.
- [45] M. E. M. K. Abdelaziz, J. Zhao, B. G. Rosa, H.-T. Lee, D. Simon, K. Vyas, B. Li, H. Koguna, Y. Li, A. A. Demircali, H. Uvet, G. Gencoglan, A. Akcay, M. Elriedy, J. Kinross, R. Dasgupta, Z. Takats, E. Yeatman, G.-Z. Yang, and B. Temelkuran, “Fiberbots: Robotic fibers for high-precision minimally invasive surgery,” *Science Advances*, vol. 10, no. 3, p. eadj1984, 2024.
- [46] H. Mori, S. Torii, M. Kutyna, A. Sakamoto, A. V. Finn, and R. Virmani, “Coronary artery calcification and its progression: What does it really mean?,” *JACC: Cardiovascular Imaging*, vol. 11, no. 1, pp. 127–142, 2018.
- [47] M.-S. Kim, S.-J. Kang, C.-W. Lee, S. Han, D.-W. Park, S.-W. Lee, Y.-H. Kim, S.-W. Park, S.-J. Park, and J.-J. Kim, “Prevalence of coronary atherosclerosis in asymptomatic healthy subjects: An intravascular ultrasound study of donor hearts,” *Journal of Atherosclerosis and Thrombosis*, vol. 20, no. 5, pp. 465–471, 2013.
- [48] E. M. Tuzcu, S. R. Kapadia, E. Tutar, K. M. Ziada, R. E. Hobbs, P. M. McCarthy, J. B. Young, and S. E. Nissen, “High prevalence of coronary atherosclerosis in asymptomatic teenagers and young adults: evidence from intravascular ultrasound,” *Circulation*, vol. 103, pp. 2705–2710, June 2001.
- [49] O. M. McGee, W. Sun, and L. M. McNamara, “An in vitro model quantifying the effect of calcification on the tissue–stent interaction in a stenosed aortic root,” *Journal of Biomechanics*, vol. 82, pp. 109–115, 2019.
- [50] K. Takashima, R. Shimomura, T. Kitou, H. Terada, K. Yoshinaka, and K. Ikeuchi, “Contact and friction between catheter and blood vessel,” *Tribology International*, vol. 40, no. 2, pp. 319–328, 2007. First International Conference on Advanced Tribology (iCAT 2004).
- [51] P. S. Yarmolenko, E. J. Moon, C. Landon, A. Manzoor, D. W. Hochman, B. L. Viglianti, and M. W. Dewhirst, “Thresholds for thermal damage to normal tissues: An update,” *International Journal of Hyperthermia*, vol. 27, no. 4, pp. 320–343, 2011. PMID: 21591897.
- [52] N. B. D. Do, E. Andreassen, S. Edvardsen, A. Lifjeld, K. E. Aasmundtveit, H.-V. Nguyen, and K. Imenes, “Thermal management of an interventional medical device with double layer encapsulation,” *Experimental Heat Transfer*, vol. 35, no. 5, pp. 708–725, 2022.
- [53] N. Xiao, J. Guo, S. Guo, and T. Tamiya, “A robotic catheter system with real-time force feedback and monitor,” *Australasian physical & engineering sciences in medicine*, vol. 35, no. 3, p. 283–289, 2012.
- [54] J. A. Greenwood and J. P. Williamson, “Contact of nominally flat surfaces,” *Proceedings of the royal society of London. Series A. Mathematical and physical sciences*, vol. 295, no. 1442, pp. 300–319, 1966.
- [55] A. Bush, R. Gibson, and T. Thomas, “The elastic contact of a rough surface,” *Wear*, vol. 35, no. 1, pp. 87–111, 1975.
- [56] B. N. J. Persson, “Relation between interfacial separation and load: A general theory of contact mechanics,” *Phys. Rev. Lett.*, vol. 99, p. 125502, Sep 2007.
- [57] W. Langlois, “Isothermal squeeze films,” *Quarterly of Applied Mathematics*, vol. 20, no. 2, pp. 131–150, 1962.
- [58] M. Mediouni, T. Kucklick, S. Poncet, R. Madiouni, A. Abouaomar, H. Madry, M. Cucchiarini, B. Chopko, N. Vaughan, M. Arora, K. Gökkuş, L. P. C. Mario Lozoya Lara, A. Volosnikov, M. Hesmati, and K. Ho, “An overview of thermal necrosis: present and future,” *Current Medical Research and Opinion*, vol. 35, no. 9, pp. 1555–1562, 2019.